# Experimental studies on coherent synchrotron radiation at an emittance exchange beamline

J. C. T. Thangaraj,* R. Thurman-Keup, J. Ruan,
A. S. Johnson, A. H. Lumpkin, and J. Santucci
*Fermi National Accelerator Laboratory, Batavia, Illinois 60510 U. S. A*

(Dated: March 6, 2012)

## Abstract

One of the goals of the Fermilab A0 photoinjector is to experimentally investigate the transverse to longitudinal emittance exchange (EEX) principle. Coherent synchrotron radiation in the emittance exchange line could limit the performance of the emittance exchanger at short bunch lengths. In this paper, we present experimental and simulation studies of the coherent synchrotron radiation (CSR) in the emittance exchange line at the A0 photoinjector. We report on time-resolved CSR studies using a skew-quadrupole technique. We also demonstrate the advantages of running the EEX with an energy chirped beam.

* jtobin@fnal.gov

## I. INTRODUCTION

The ability to manipulate the 6-D phase-space of the electron beam is important for both modern and future accelerators. One such phase-space manipulation scheme involves exchanging the longitudinal emittance with the transverse emittance of the beam. The ability to exchange emittances could be useful in free electron lasers, where exchanging the larger transverse emittance with the smaller longitudinal emittance can help suppress the microbunching instability [1]. At the Fermilab A0 photoinjector, a proof-of-principle experiment of an emittance exchange scheme has been demonstrated recently [2]. The emittance exchange line consists of a $TM_{110}$ cavity sandwiched by doglegs, a variation of the original scheme proposed by Cornacchia and Emma [3], where the cavity was in the middle of a chicane. Neither scheme takes into account collective effects such as space-charge, coherent synchrotron radiation, and wakefields.

Our goal in this work is to investigate coherent synchrotron radiation effects (CSR) in the emittance exchange line. Synchrotron radiation is the electromagnetic radiation emitted by an accelerated charged particle. CSR refers to synchrotron radiation with a wavelength that is longer than the bunch length and thus emited coherently throughout the bunch[4]. At the A0 photoinjector, the CSR originates from the dipole bending magnets in the dogleg sections. The intensity of CSR scales as $N^2$, where $N$ is the number of particles in the bunch. The power loss due to CSR can be expressed as [5]: $P = \frac{N^2 x e^2}{\epsilon_0 \rho^{2/3} \sigma_z^{4/3}}$ Watts, where $N$ is the number of particles, $x$ is 0.0279, $\rho$ is the bending radius , $\sigma_z$ is the bunch length, and $e$ is the charge of electron. Therefore, the shorter the bunch at the dipole, the larger the power loss due to CSR. In addition to the average energy loss, the radiation from the tail of the bunch can catch up with the head of the bunch and interact leading to an energy spread within the bunch. The energy spread is then converted to an emittance growth when the bunch exits the bend which may lead to imperfect emittance exchange. Some recent experimental works on CSR in a chicane are in references [6–8].

In this paper we begin with the measurement of CSR power as a function of charge and bunch length, followed by a report on the measurement of the angular distribution and polarization of the CSR. We then show how CSR was used to measure the bunch length of the electron beam and compare with numerical simulations. Next we show results from time-resolved studies of CSR using a skew quadrupole. Finally we conclude with measurements

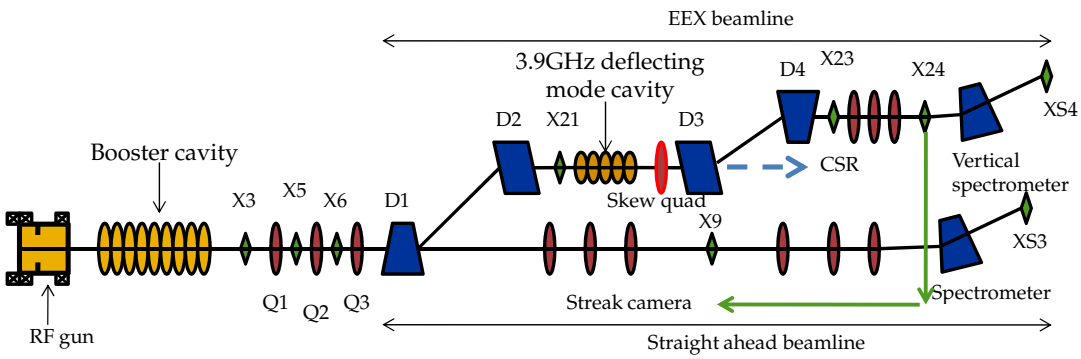


FIG. 1. Experimental setup of the A0 photoinjector facility. Electrons generated by the RF gun are accelerated through the booster cavity to 14 MeV. Q1, Q2, Q3 focus the beam before it enters the EEX beamline. D1, D2, D3 and D4 are the dipole magnets. The skew quadrupole located before D3 is used to study time-resolved effects. X# refers to beam imaging stations.

from the emittance exchanger, where a peak current increase by a factor of 2 was obtained with an energy-chirped beam.

## II. EXPERIMENTAL SETUP

The A0 photoinjector facility (A0PI) shown in Fig. 1 consists of an L-band RF gun followed by a superconducting 9-cell booster cavity, which accelerates the electron beam up to 16 MeV. After acceleration, the beam is steered and focused using the dipoles and the quadrupoles (Q1 Q2 Q3). The beam can either continue straight to XS3 or be steered into the dogleg. In our experiments, the beam is sent through the doglegs to the spectrometer (XS4). Located between the doglegs is the liquid-nitrogen-cooled, 5-cell 3.9 GHz $TM_{110}$ deflecting mode cavity, which was switched on/off during our study. When the bunch passes through the dogleg, CSR is expected to be more pronounced at dipole D3. So, we installed optics to collect the radiation coming out of the port at dipole D3. The light is collimated using an off axis parabolic mirror onto a plane mirror. The reflected light is then directed either to a single $LiTaO_3$ crystal pyrodetector (for power measurement) or to a Martin-Puplett interferometer (to measure bunch length). The layout of the collecting optics is shown in Fig. 2.

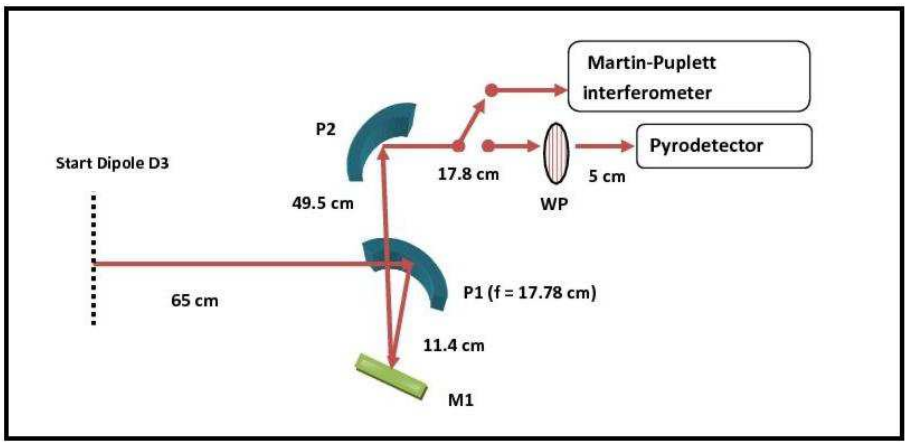


FIG. 2. Schematic of the synchrotron light collection optics from dipole D3. CSR is first collected by an off-axis parabolic mirror (P1 with focal length = 17.78 cm) and focussed on a mirror (M1) which reflects the light to another parabolic mirror (P2). P2 focuses the light onto a pyrodetector or a Martin-Puplett interferometer. The wire-grid polarizer (WP) was installed 5 cm before the pyrodetector.

### A. CSR Power measurements

Since the bend plane is horizontal in the doglegs, the synchrotron radiation is predominantly horizontally polarized. The total emitted power, P, can be shown to be equal to: $P = NP_{inc}(1 + Ng(\lambda))$where $P_{inc}$ is the single particle classical synchroton radiation power, $N$ is the number of particles and $g(\lambda)$ is the form factor proportional to the Fourier transform of the longitudinal profile of the bunch. If the condition for coherency is satisfied i.e. $Ng(\lambda) >> 1$, the single particle radiation intensity is multiplied by the bunch form factor and $N^2$ to yield CSR. For a Gaussian bunch with rms bunchlength $\sigma_z$ the form factor $g(\lambda) = exp[-(\frac{2\pi\sigma_z}{\lambda})^2]$, indicating that bunches will emit CSR at wavelengths longer than $2\pi\sigma_z$.

We measured the intensity of the radiation for various bunch charges and at different RF phases. We found that the detector power is maximum at the minimum bunch length for a fixed charge, as expected from the theory. Moreover, the detected power also varies quadratically with charge as expected from coherent radiation and this is shown in Fig. 3. Comparison between charges with a fixed number of bunches in a bunch train poses

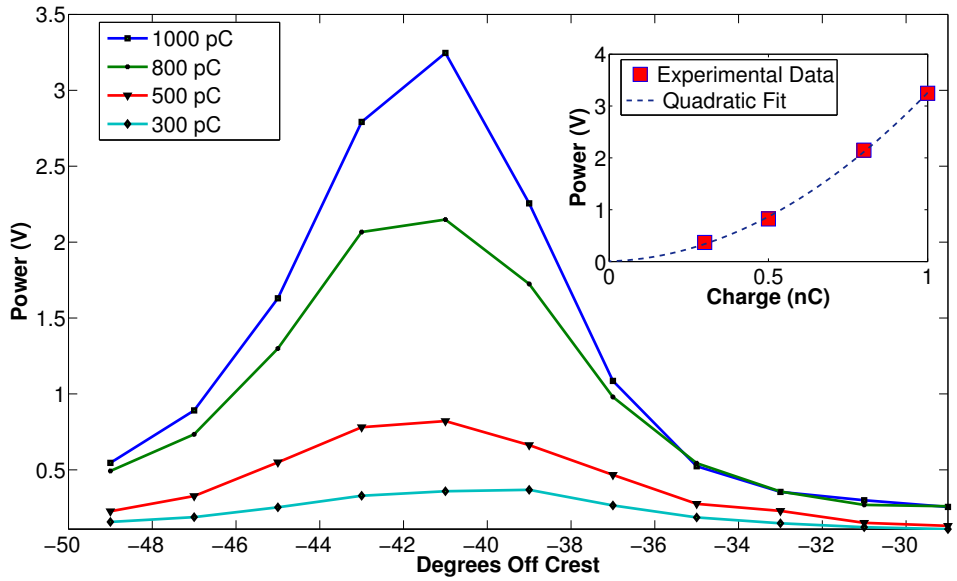


FIG. 3. CSR Power measurement at D3 as a function of 9-cell booster cavity phase. Maximum power is observed at 41° off crest. The inset shows the fit of the CSR power as a function of charge.

a limitation because the pyrodetector is saturated for higher charge at a lower number of bunches. The number of bunches we chose was 10 to prevent the pyrodetector from saturating at 1 nC.

As seen in Fig. 3, the CSR power peaks at 41° off-crest, and this feature can be explained as follows. The final bunchlength, $\sigma_{zf}$, of the beam after going through a bend system is $\sigma_{zf} = \sqrt{(1+\kappa R_{56})^2\sigma_{zi}^2 + (R_{56}\sigma_{\delta_i})^2}$, where $\sigma_{zi}$ is the initial bunchlength, $\sigma_{\delta_i}$ is the initial energy spread, $R_{56}$ is the longitudinal dispersion and $\kappa$ is the linear chirp. To minimize the bunch length, we must minimize the incoming energy spread and/or set the linear chirp of the RF 9-cell booster cavity to $\kappa = -\frac{1}{R_{56}}$. For the bending system (first dogleg alone in our case), $R_{56}$=0.12 m, so the chirp should be $\kappa$=8.33. For this chirp, the RF phase corresponds to $\phi$=23°. Normally, to minimize the energy spread introduced by the electron gun, the RF phase is set to $\sim \phi_0 = 23°$ ($\kappa$=8.33). At this value of the RF phase, the beam has no chirp. So, in order to compress we introduce an RF chirp on top of the regular offset phase. In other words, we should operate the 9-cell phase at a total chirp, $\kappa = 16.6$. This value of chirp is obtained for an RF phase off-crest value of $\phi = 40$, which agrees well with the observed values.

### B. Polarization and Angular distribution of CSR

A wire-grid polarizer, which could be remotely rotated, was installed in front of the pyrodetector. The grids consist of 15 $\mu$m diameter tungsten wires spaced by 45 $\mu$m. The intensity of the CSR was measured as a function of the polarizer angle and is shown in Fig. 4 along with a fit function. As expected, the light is mostly horizontally polarized. Assuming an electric field $\overrightarrow{E_x}$ and $\overrightarrow{E_y}$ for the horizontal and the vertical polarization components, incident at an angle of $\theta$ at the polarizer, the electric field after the polarizer is given by $\overrightarrow{E_t} = \overrightarrow{E_x}\cos\theta + j\overrightarrow{E_y}sin\theta$. So, the intensity at the detector is $|E_t|^2 = \overrightarrow{E_t}.\overrightarrow{E_t^*} = E_x^2\cos^2\theta + E_y^2\sin^2\theta$.

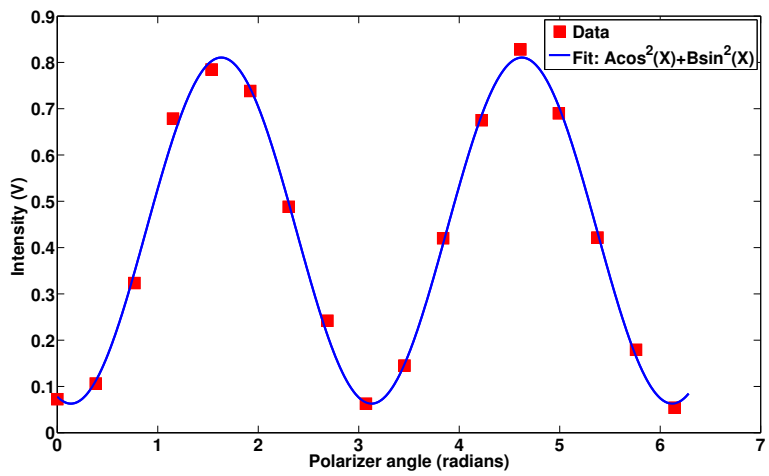


FIG. 4. The measured CSR intensity as a function of polarizer angle. While the sinusoidal behavior indicates a horizontally polarized CSR light, the non-zero baseline indicates the vertical polarization component of the CSR.

To map the angular distribution of the light, the detector was mounted on an X-Y translation stage and scanned over an area of 55 mm x 60 mm with a 5-mm step size in each direction. The measurement was done for both horizontal and vertical polarizations, as shown in Fig. 5. The measured ratio between the horizontal and the vertical polarization components was 4.6. Theoretically, the horizontal polarization carries 7 times more power than the vertical [9] . The difference may be due to several factors: the theory assumes the collection of all frequencies over all angles, while in the experiment we are limited by the finite size of the detector, finite geometry of the beam pipe cutting off some frequencies, and the diffraction limitation of the relay optics [10]. Also, shown in Fig. 5 is a slice of

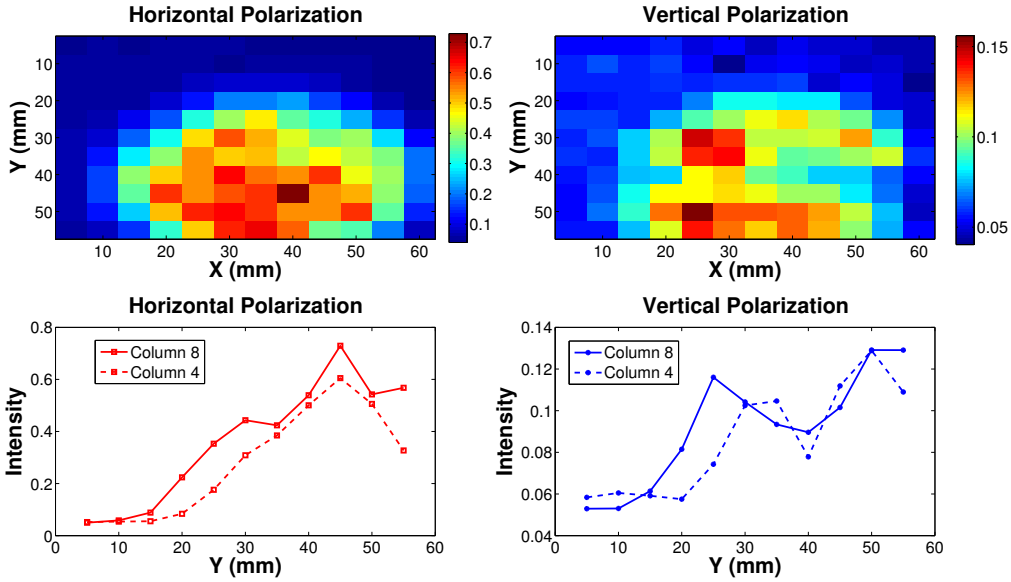


FIG. 5. Top: Measured angular distribution of the CSR radiation with horizontal polarization (left) and with vertical polarization (right). Bottom: Two slice projections from the spatial distribution showing the angular distribution of the coherent synchrotron radiation. The horizontal polarization (left) shows a maximum at the center - a single lobe, while the vertical polarization (right) shows a dip in the center - a double-lobed feature. Note: the scales are different by a factor of ∼5 indicating higher intensity of the horizontally polarized synchrotron radiation.

the spatial distribution showing the angular distribution of the CSR. The dip in the vertical angular distribution of the classical synchrotron radiation is observed. The vertical dip does not go to zero possibly due to the finite energy spread and divergence in the beam.

### C. Bunch-length measurements

Coherent synchrotron radiation carries the bunch profile information of the electron beam in its bunch form factor. In order to extract the bunch length, the CSR was directed into a Martin-Puplett interferometer. A Martin-Puplett interferometer is a polarizing type interferometer. The incoming light is first sent through a horizontal polarizer. Then, the horizontally polarized light wave is split using a beam splitter and directed to their respective arms of the interferometers. Once split, the light waves travel toward the roof mirror, which changes the polarization of the waves, and reflects them back to the beam splitter, where

they are recombined. The recombined waves are again split and sent to pyrodetectors. The pyrodetector signals are digitized and read by a MATLAB routine. After choosing an appropriate fitting model in the program, the bunch length is calculated [11]. The results of the measurements and a comparison with the single-particle simulation using both *BeamLattice* [12] - a program based on a linear matrix model - and *elegant* [13] are shown in Fig. 6. The uncertainty in the measurement is primarily due to the choice of the fitting function used to best capture the low-frequency cut-off of the detector. Simulation agrees with the experimental value for shorter bunch length while at longer bunch lengths low-frequency diffraction effects dominate, leading to the discrepancy. Also, the predicted RF phase at which the bunch length is minimum shows good agreement with the experimental value.

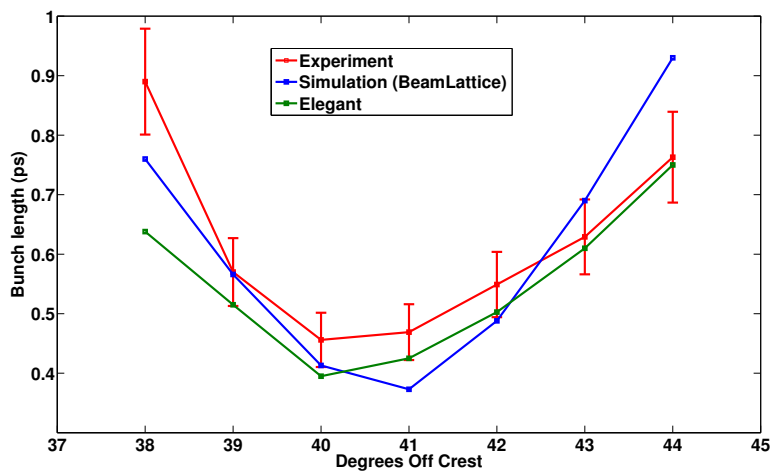


FIG. 6. R.M.S. bunch length comparison between *elegant* simulation including CSR, single-particle matrix-simulation without CSR, and the measurements.

### D. Skew quadrupole

Motivated by the work at SLAC that used a skew quadrupole to study CSR effects in a bunch compressor [14], a skew quadrupole was installed before the dipole D3. At the skew quadrupole, the particle gets a $y$-kick proportional to its $x$-position, $y' = \frac{x}{F}$ where $F$ is the focal length of the skew quadrupole. This kick is converted to a y-position change at the screen downstream of the exchanger at X24: $y_{screen} = R_{34} y'_{quad}$ . The subscript

quad indicates the skew quadrupole. In terms of r.m.s. quantities, as long as the $\beta_y$ at the screen is small, the y-beamsize at the screen is $\sigma_{y_{screen}} = \frac{\sigma_{x\,quad}}{K}$, where $K$ is a constant and $\sigma_{xquad} = \sqrt{x_{\beta quad} + (\eta_x \sigma_\delta)^2}$, where $\eta_x$ is the dispersion and $\sigma_\delta$ is the r.m.s energy spread. We consider two cases: with and without the 5-cell cavity powered.

*1.* WITH 5-CELL OFF:

If the beam size at the skew quadrupole is dominated by the dispersion term (as in a bunch compressor) and assuming linear chirp $h$, ($\sigma_\delta = h\sigma_{z_{in}}$), we can write: $\sigma_{y_{screen}} = \frac{h\sigma_{z_{in}}}{K}$. After cancelling dispersion, the $\sigma_{y_{screen}}$ is proportional to incoming bunch length. In our setup, the dispersion is cancelled by using the last three quads after the X23 screen station.

*2.* WITH 5-CELL ON:

If the 5-cell is on and the RF chirp is zero (at minimum energy spread), then we can write $y_{screen} = \frac{\sqrt{x_{\beta quad}}}{K} \propto \frac{\sqrt{{x_0}^2 + L{x_0'}^2}}{K}$ , where L is the length of the dogleg drift, because the beam size at the skew quadrupole is now dominated by $\beta_x$. From EEX transport equations [2], we can write $\delta_{out} = \frac{-x_0}{\eta} - \frac{Lx_0'}{\eta}$, where $x_0$ and $x_0'$ are the inital transverse x-position and the angle of the beam before the EEX. Also, for a single particle going through a dogleg (with no chirp), $x_{quad} = x_0 + Lx_0'$. Hence, we can write $x_{quad} = \delta_{out}\eta$. In summary, when the chirp is zero and with the 5-cell on, the y-beam size maps the outgoing energy profile: $y_{screen} \propto \frac{\delta_{out}\eta}{\kappa_0}$, where $\kappa_0$ is a constant of proportionality. Thus, the skew quadrupole acts like a vertical spectrometer. We note that we have made a thin-lens approximation for the 5-cell and have ignored effects like space charge. Also, we have made an assumption that the time and energy are linearly correlated at the accelerating cavity, which is not exactly true if the operating phase is close to the crest. In our case, since we are far off-crest, this is not a bad approximation.

### E. 5-cell off: Twin pulse transport

To begin our study, we used two electron pulses separated in time ($\sim$ 11 ps) and then turned on the skew quadrupole to see whether the time separation between the pulses

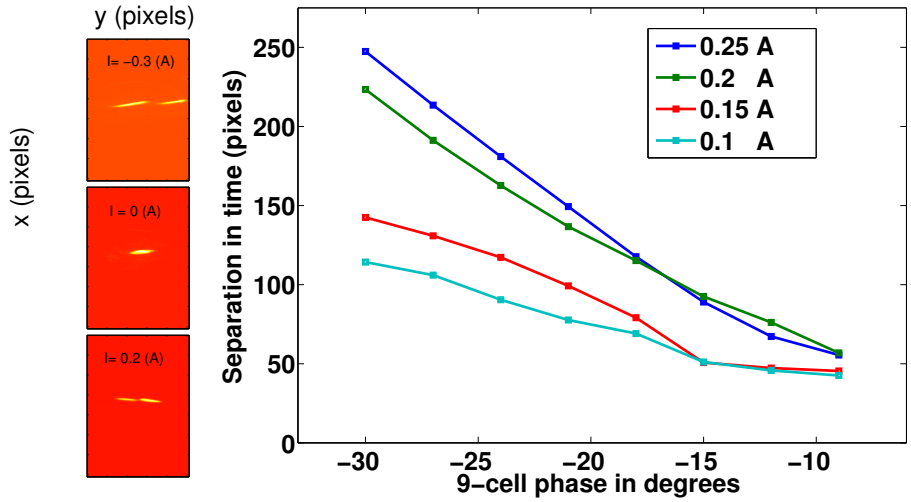


FIG. 7. The figures on the left show the transverse images of the twin pulses observed at X24 versus the skew quadrupole current in Amps. When the skew quadrupole is turned on, the separation in pulses is observed. On the right, the time separation of the pulses in time (in pixel units) are given as a function of RF chirp for every skew quadrupole strength. Each pixels is equal to 32.8 microns.

could be revealed on the screen. The electron pulses separated in time experience different accelerating fields in the 9-cell and end up with different energies, but this does not show a x-position change at X24 because the dispersion is cancelled at X24 using the quads before X24. By turning on the skew quadrupole, dispersion couples to the y-plane - thereby acting like a vertical deflector as shown in Fig. 7. As the skew quadrupole changes sign, the pulses flip their positions showing a direct correlation between the skew-quadrupole strength and time-resolution at a fixed RF chirp. Also we find that the larger the chirp, the more sensitive the time resolution is for a fixed skew current. Thus the skew quadrupole can be used to time resolve the $x$-beamsize at X24.

### F. 5-cell turned on: Slit-based measurements

In order to study the effect of the skew quadrupole on the emittance exchange line, we switched on the 5-cell with the vertical slits inserted at X3. When the slits are inserted, the transverse modulation is transfered to longitudinal phase space leading to an energy

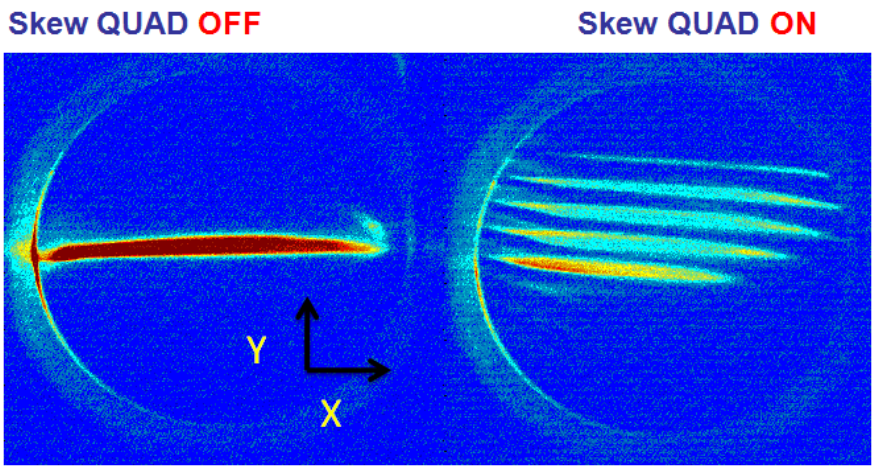


FIG. 8. Measured transverse beam images at X23 with the slits in at X3 and the 5-cell turned on. The skew quadrupole projects the energy spectrum on the screen when the chirp is zero due to the leakage of the horizontal dispersion to the vertical plane. The observed separation of the slits in the y-direction is in good agreement with the simulation shown in Fig. 9.

and time modulation [15]. Hence at X23, the beam image has no modulation. But, when the skew quadrupole was turned on, the modulation effects are visible in the y-direction, as shown in Fig. 8 and can be explained as follows: when the chirp is zero (at minimum energy spread), the $x$-beamsize at the skew quadrupole is dominated by $\beta_x$ and hence the skew quadrupole projects the $x$-modulation in $y$ at the screen. Any chirp then shows itself as the slit orientation at X23. However, the $x$-modulation at the skew quadrupole is proportional to the energy modulation at the output of the 5-cell. Hence, the skew quadrupole can be used to measure the energy spectrum of the beam exiting the EEX. This is consistent with the simulation results from *BeamLattice* as shown in Fig. 9

### G. Simulations

We used *BeamLattice* and *elegant* programs to study the effect of the skew quadrupole on beam dynamics. After optimizing the beta-function using *elegant*, we turned on CSR effects in *elegant* by introducing CSRSCBEND and CSRDRIFT elements. The results are shown in Fig. 10. The signature of the CSR wake potential is clearly visible in the simulations.

CSR modulates the energy by accelerating the head of the bunch which results in a

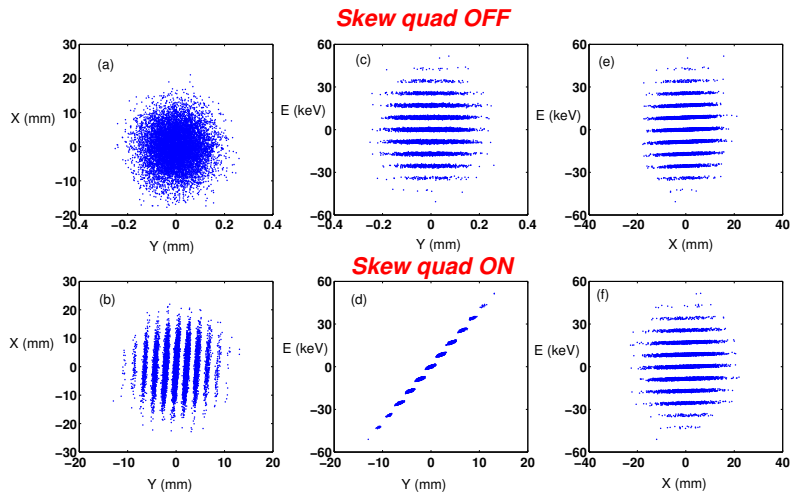


FIG. 9. *BeamLattice* results showing the effect of the skew quadrupole at X23 with slits in at X3 and 5 cell on. Fig. (a) and (b) shows X vs Y transverse dimensions with the skew quadrupole off and on. Fig. (c) and Fig. (d) shows Energy vs Y with the skew quadrupole off and on. Turning on the skew quadrupole couples dispersion in the vertical plane introducing a strong correlation between E and Y as shown in Fig. (d) which is mapped on the screen thus acting as a vertical spectrometer [Fig. (b)]. The x vs E plane shown in Fig. (e) and Fig. (f) is un-affected by turning on the skew quadrupole.

change in the transverse positions of the particles as they exit the bend. The measured image profile at X24 for various charges with and without the skew quadrupole on is shown in Fig. 11. As the charge increases, the CSR "bulge" effect is seen on the screen as shown in Fig. 11. This is consistent with the CSR power measurement in Fig. 3, where increase in charge shows a quadratic increase in CSR power loss indicating that the CSR effect is more pronounced at higher charges. Here we have made a thin-lens approximation for the 5-cell and have ignored other collective effects like space charge and wakefields.

## III. BUNCH COMPRESSION

In all our experiments mentioned above to measure CSR, we had to impart an energy chirp on the beam using the 9-cell accelerating cavity. We show in this section that running the emittance exchanger (which is typically run with no energy chirp) with an energy-chirped beam has advantages.

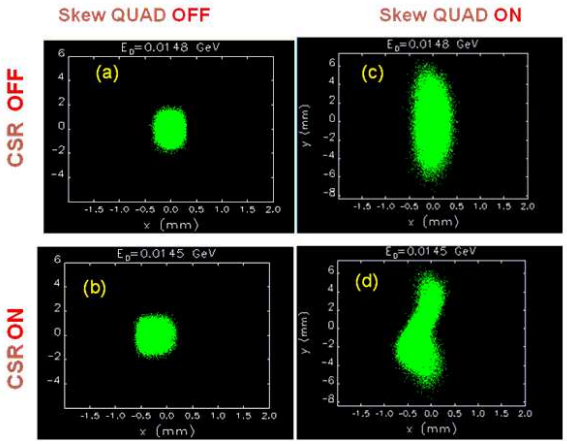


FIG. 10. *elegant* simulation showing the effect of CSR and skew quadrupole at X24 with 5-cell off. Fig. (a) shows the both CSR and the skew quadrupole off. When there is no CSR, the skew quadrupole acts like a vertical deflector as showin in Fig. (c). Due to CSR, the head particles gain energy leading to a transverse offset as shown in Fig. (d). Fig. (b) shows the case with the skew quadrupole off and CSR on.

In the emittance exchange beamline, if we assume a thick lens for the cavity, the transfer matrix is altered with coupling from incoming $z$ and $\delta$ [2]. So, the outgoing particle $z_2 = \kappa\xi x_1 + \left[\frac{-1}{\kappa} + \left(\frac{L_c}{4} + L\right)\xi\right]\kappa x_1' + \frac{L_c\kappa^2\xi}{4}\left(z_1 + \xi\delta_1\right)$ where $\xi$ is the longitudinal dispersion, $x_1, x_1', z, \delta$ are the incoming x-position, x-angle, longitudinal position, energy spread of the beam and $L_c, L, \kappa$ are the length of the cavity, the length of the dogleg and the strength of the cavity respectively. If we set the chirp $= \frac{\delta_1}{z_1} = \frac{-1}{\xi}$, then the last term in the equation will be zero or minimized [1, 16].

During the emittance exchange experiment, the beam injected into the EEX beamline has no chirp. We impart a chirp on the beam by operating the 9-cell off-crest and measure the bunch length of the electron beam at X24 with a streak camera. For Q3 between 0.35 to 0.55, the bunchlength reached the resolution limit of the streak camera ($\sim$300 fs) as shown in Fig. 12. We then did power measurements with both the bolometer and the pyrodetector for a beam with and without chirp, as shown in Fig. 13. The results indicated a factor of 2 increase in the power detected for a beam with RF chirp. There were 60 bunches and the 5-cell was on in both the cases.

These results motivated us to operate the EEX beamline with a chirp for the beam and to use the Martin-Puplett interferometer for the bunch length measurement. The CTR

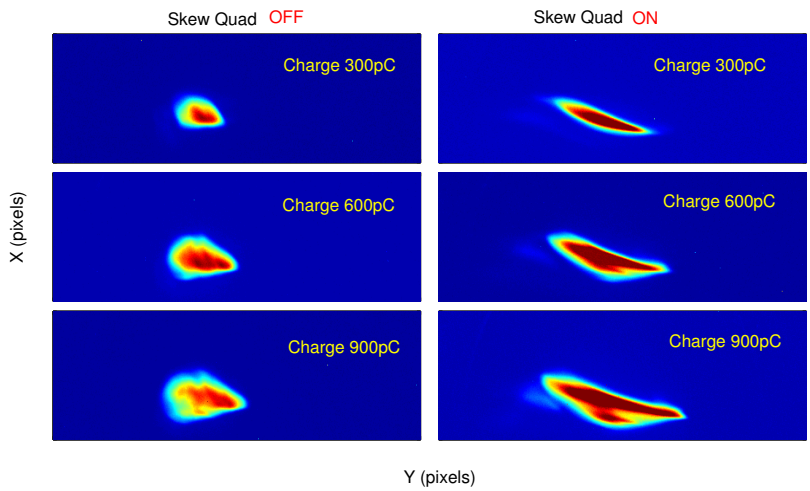


FIG. 11. Measured transverse beam profile at X24 as a function of skew quadrupole off (left column) and skew quadrupole on (right column) for various charges. The CSR bulge effect is prominent at higher charges. The image is rotated by $90^0$ compared to Fig. 10. When the skew quadrupole is turned on, the y-axis on the right is proportional to the incoming bunchlength and x-axis proportional to the energy. Each image is 600 pixels x 150 pixels with each pixels measuring 32.8 microns.

radiation from X24 was used to measure the auto-correlation of the beam with and without energy chirp. The result is shown in Fig. 14. The bunch with chirp (red) shows a shorter auto-correlation width compared with the bunch with no chirp (blue). Assuming a Gaussian bunch and extracting the bunch length from the auto-correlation using the formula: $\sigma_t = \frac{FWHM_{center}}{2.35\sqrt{(2)}}$ where $FWHM_{center}$ corresponds to the full-width half maximum of the center peak, yields a bunch length of 0.60 ps (blue) and 0.25 ps (red). Therefore, adding a chirp decreases the bunch length by a factor of $\sim$2.4. In other words, the beam with an RF chirp is shorter compared to the one without chirp. This is consistent with the power measurements which also showed a factor of $\sim$2 increase in the detector power for a beam with chirp and also agrees with the theoretical predictions and computer simulations. The bunch length formula has been verified through computer simulation which assumes a Gaussian bunch along with a diamond window for the extraction port. Electro-optic sampling, which could possibly reveal the bunch profile, is also being developed as an alternative diagnostic at A0 photoinjector [17]. Further data on emittance measurements using chirped beam is currently being analyzed.

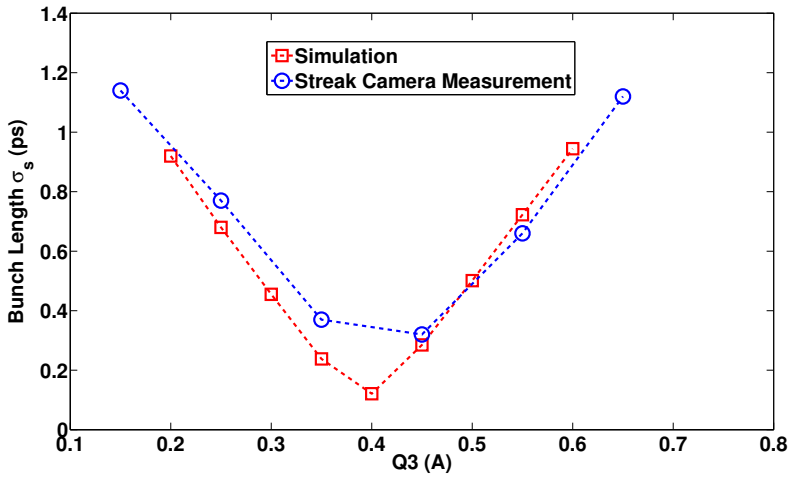


FIG. 12. Comparison of bunch lengths of the electron beam measured at X24 using a streak camera as a function of quadrupole (Q3) current versus those of simulation using *BeamLattice*. The chirp was set to -40 degrees off-crest.

## IV. SUMMARY AND CONCLUSIONS

Coherent synchrotron radiation has been generated, detected and measured from the emittance exchange beamline at the A0 photo-injector using an energy-chirped beam. The features of CSR such as the angular distribution, the intensity ratio of the horizontal to vertical polarization, and quadratic variation with charge have been presented. A time-resolved measurement of the CSR "bulge" effect has been measured using the skew-quadrupole at high charge. Finally, by operating the emittance exchange with an energy chirp, a factor of 2 enhancement in peak current has been achieved, demonstrating a possible use of emittance exchange as a bunch compressor. Preliminary results indicate that operating the emittance exchanger with an energy-chirped beam not only shows CSR effects are minimal at lower charges but results in an actual improvement in the emittance exchanger performance. This is consistent with theory and recent simulation [1, 18, 19]. Further data are being investigated to get an accurate measurement of the emittances after the beamline when operated with a significant energy chirp.

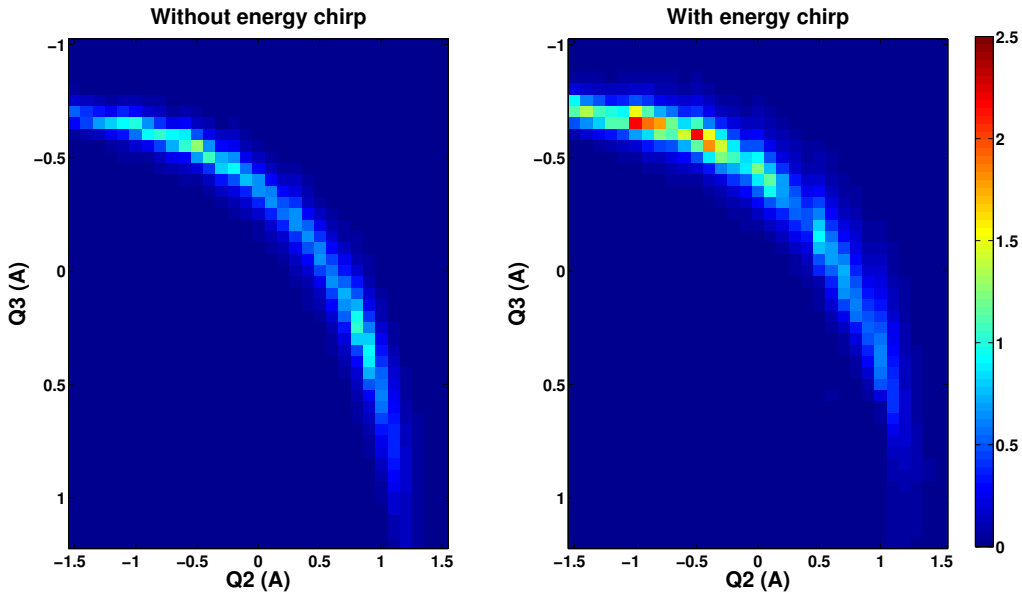


FIG. 13. Pyrodetector measurements of coherent transition radiation at X24 as a function of upstream quadrupoles Q2 and Q3. No energy chirp on the beam (left) and with an energy chirp on the beam (right) at 40 degrees off crest. The intensity obtained when the beam is chirped is a factor of 2 higher compared with the no chirp case at certain quadrupole settings.

## ACKNOWLEDGMENTS

The authors are indebted to the A0 technical support team . We thank M. Church, H. Edwards, T. Maxwell, P. Piot and Y.-E.Sun for their interest and encouragement. The work was supported by the Fermi Research Alliance, LLC under the U.S. Department of Energy.

---

[1] P. Emma, Z. Huang, K.-J. Kim, and P. Piot, "Transverse-to-longitudinal emittance exchange to improve performance of high-gain free-electron lasers," *Phys. Rev. ST Accel. Beams*, vol. 9, p. 100702, Oct 2006.

[2] J. Ruan, A. S. Johnson, A. Lumpkin, R. Thurman-Keup, H. Edwards, R. Fliller, T. Koeth, and Y. Sun, "First observation of the exchange of transverse and longitudinal emittances," *Physical Review Letters*, vol. 106, no. 24, p. 244801, 2011.

[3] M. Cornacchia and P. Emma, "Transverse to longitudinal emittance exchange," *Phys. Rev. ST Accel. Beams*, vol. 5, p. 084001, Aug 2002.

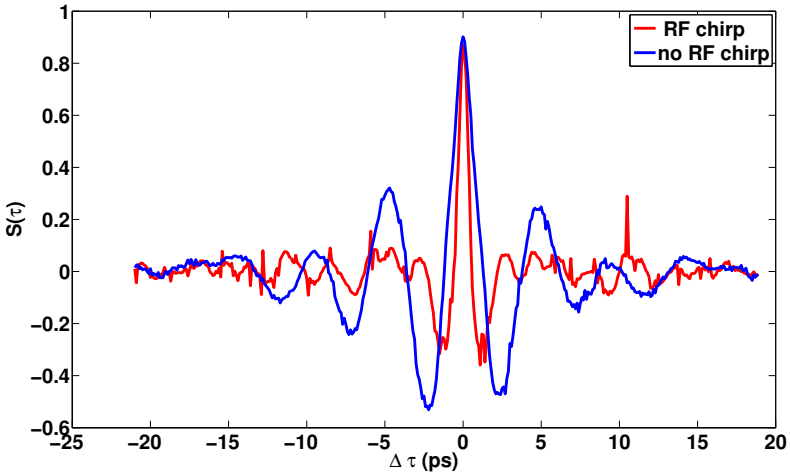


FIG. 14. Auto-correlation measurement with Martin-Puplett interferometer with and without energy chirp.


[4] J. Schwinger, "On the classical radiation of accelerated electrons," *Phys. Rev.*, vol. 75, pp. 1912–1925, Jun 1949.

[5] Y. Derbenev, J. Rossbach, E. Saldin, and V. Shiltsev, "Microbunch radiative tail-head interaction," *TESLA-FEL 95-05*, 1995.

[6] B. Beutner, *Measurement and Analysis of Coherent Synchrotron Radiation at FLASH*. DESY-THESIS-2007-040, 2007.

[7] H. H. Braun, R. Corsini, L. Groening, F. Zhou, A. Kabel, T. O. Raubenheimer, R. Li, and T. Limberg, "Emittance growth and energy loss due to coherent synchrotron radiation in a bunch compressor," *Phys. Rev. ST Accel. Beams*, vol. 3, p. 124402, Dec 2000.

[8] K. L. F. Bane, F.-J. Decker, Y. Ding, D. Dowell, P. Emma, J. Frisch, Z. Huang, R. Iverson, C. Limborg-Deprey, H. Loos, H.-D. Nuhn, D. Ratner, G. Stupakov, J. Turner, J. Welch, and J. Wu, "Measurements and modeling of coherent synchrotron radiation and its impact on the linac coherent light source electron beam," *Phys. Rev. ST Accel. Beams*, vol. 12, p. 030704, Mar 2009.

[9] H. Wiedemann, *Synchrotron radiation*. Springer Verlag, 2003.

[10] G. Carr, M. Martin, W. McKinney, K. Jordan, G. Neil, and G. Williams, "High-power terahertz radiation from relativistic electrons," *Nature*, vol. 420, no. 6912, pp. 153–156, 2002.

[11] R. Thurman-Keup, R. Fliller, and G. Kazakevich, "Bunch length measurement at the Fermilab A0 photoinjector using a martin-puplett interferometer," *Proceeding of Beam Instrumentation Workshop BIW08*, 2008.

[12] An in-house software based on TRACE3D linear matrix model for beam transport with a GUI interface. This code was written in MATLAB by R. Thurman-Keup.

[13] M. Borland, "elegant: A flexible sdds-compliant code for accelerator simulation," *Advanced Photon Source LS-287*, 2000.

[14] K. Bertsche, P. Emma, and O. Shevchenko, "A simple, low cost longitudinal phase space diagnostic," *SLAC-PUB-13614*.

[15] Y.-E. Sun, P. Piot, A. Johnson, A. H. Lumpkin, T. J. Maxwell, J. Ruan, and R. Thurman-Keup, "Tunable subpicosecond electron-bunch-train generation using a transverse-to-longitudinal phase-space exchange technique," *Phys. Rev. Lett.*, vol. 105, p. 234801, Dec 2010.

[16] B. Jiang, J. G. Power, R. Lindberg, W. Liu, and W. Gai, "Emittance-exchange-based high harmonic generation scheme for a short-wavelength free electron laser," *Phys. Rev. Lett.*, vol. 106, p. 114801, Mar 2011.

[17] T. Maxwell, P. Piot, J. Ruan, and R. Thurman-Keup, "Single-shot electro-optic sampling of coherent transition radiation at the a0 photoinjector," *Proceedings of the International Particle Accelerator Conference (IPAC 2011)*, 2011.

[18] B. E. Carlsten, K. A. Bishofberger, S. J. Russell, and N. A. Yampolsky, "Using an emittance exchanger as a bunch compressor," *Phys. Rev. ST Accel. Beams*, vol. 14, p. 084403, Aug 2011.

[19] A. Zholents and M. Zolotorev, "A new type of bunch compressor and seeding of a short wave length coherent radiation," *Advanced Photon Source ANL/APS/LS-327*, 2011.